

The seismic purifier: An unsupervised approach to seismic signal detection via representation learning

Onur Efe*, Arkadas Ozakin†

Bogazici University, Department of Physics

*onur.efe@boun.edu.tr , †arkadas.ozakin@boun.edu.tr

Abstract—In this paper, we develop an unsupervised learning approach to earthquake detection. We train a specific class of deep auto-encoders that learn to reproduce the input waveforms after a data-compressive bottleneck, and then use a simple triggering algorithm at the bottleneck to label waveforms as noise or signal.

Our approach is motivated by the intuition that efficient compression of data should represent signals differently from noise, and is facilitated by a time-axis-preserving approach to auto-encoding and intuitively-motivated choices on the architecture and triggering.

We demonstrate that the detection performance of the unsupervised approach is comparable to, and in some cases better than, some of the state-of-the-art supervised methods. Moreover, it has strong *cross-dataset generalization*. By experimenting with various modifications, we demonstrate that the detection performance is insensitive to various technical choices made in the algorithm.

Our approach has the potential to be useful for other signal detection problems with time series data.

Index Terms—Deep learning, neural networks, seismic signal, unsupervised learning, representation learning, waveform classification

I. INTRODUCTION

Seismic waveform classification is one of the major problems in computational seismology with a broad range of applications. Historically, classical signal detection algorithms have been used for discriminating noise from seismic events, but recent advances in machine learning have enabled supervised learning-based deep learning methods to outperform such classical methods on various datasets. Mousavi et al. [2020], Soto and Schurr [2021], Woollam et al. [2019], Zhu and Beroza [2019], Ross et al. [2018] Some of these supervised methods were shown to result in improved detection performance for events with lower magnitudes and SNRs, with very good overall performance metrics. Mousavi et al. [2020] However, evaluating the performance of such methods can be tricky due to a dependence on the specifics of the training and testing datasets. A recent review article reports significant performance variations for some of the major models from recent literature when evaluated over a range of training and testing datasets. Münchmeyer et al. [2022]

This variation of performance is related to the problem of overfitting, and is a sign of the trained models’ difficulties with generalization. Two common causes of this behavior are the specific distribution of the waveforms included in the training set, and the particular techniques used for creating the labels. Although the problem can be fixed to some degree by using bigger and more diverse datasets, there are limits to this due

to the difficulty of creating accurate training labels, which is normally done using less powerful classical algorithms and/or time-consuming human labor. Therefore, developing alternative methods that are less reliant on high-quality labels is a useful avenue of research with potentially high impact.

Unsupervised learning methods do not require labeled data, so can be used on much larger (and “cheaper”) datasets, but in their simplest form, they solve problems other than labeling and classification. Some of the most prominent problems where unsupervised learning shines are clustering, density estimation, and dimensionality reduction.

However, techniques of unsupervised learning may also be utilized on classification problems. In the context of seismological event classification, one possible approach is to use unsupervised learning to separate waveforms into clusters by using some measure of similarity (e.g. in frequency space, or some other representation) without referring to any labeling information. Once the clusters are obtained by the model, one can inspect examples from each to see if these clusters naturally/cleanly separate into noise waveforms and waveforms of different kinds of seismic events. (This can be done by using a labeled subset of the training data.) If they do, there can be hope that the cluster memberships reported by the model can be used for classification purposes. While this approach has some conceptual promise, recent work along these lines has not resulted in methods with demonstrated generalization capabilities.

Another approach to using unsupervised learning in seismological event classification involves using techniques of dimensionality reduction to find low-dimensional representations of waveforms. Starting with such representations, one can use either an additional layer of supervised learning for classification, or resort to clustering-based approaches as above to extract classes.

Works along these lines have resulted in many interesting results as we summarize below; however, it has not yet been possible to construct an “unsupervised classifier” that is capable of (1) producing labels with state-of-the-art performance metrics, and (2) generalizing to datasets significantly different from the training set.

In this paper, we propose a new unsupervised learning method we call the “seismic purifier”. Two intuitive ideas/observations motivate our approach:

- Modern techniques of “representation learning” are often capable of creating highly compressed versions of data in a way that enables one to reliably reconstruct the real

information content of a signal. Original, raw data may be high-dimensional and may contain lots of irrelevant detail, but a good model can create a low-dimensional representation that encodes only the relevant, meaningful bits.

- Seismic events are time-localized. For small events, it may be hard to distinguish a seismic signal arrival from a random fluctuation by using simplistic measures of amplitude variation, however, if one believes that there are intrinsic differences between pure noise and signal, one can imagine observing a waveform not in its raw form but in a form that represents its time-dependent “meaningful content”. Time variations in such a representation may be much more capable of accurately signaling onsets of seismic events, without being confused by meaningless fluctuations due to pure noise.

Classical methods such as STA/LTA and template matching can be seen as incarnations of the second idea in terms of very specific measures of “meaningful content”: The former being the simple power ratio in two time windows of different sizes, the latter being the time-dependent correlation with a given template waveform.

Our approach consists of combining the two ideas above using an additional ingredient. Namely, we propose to

- Train an unsupervised deep learning model to learn a low-dimensional representation of seismic signals in a way that efficiently compresses information
- Do this compression in a way that *respects the time direction*, in the sense that one dimension of the reduced representation *continues to correspond to a temporal axis*
- Use a simple/basic thresholding technique along this temporal axis of the reduced data for label waveforms as events or noise.

The intuition is simple: If the presence of an event in a waveform is indicated by a temporal change in information content, and if information is encoded efficiently in terms of a set of “signal basis directions”, then simple temporal changes along these directions should suggest the presence of events.

The success of this philosophy will in general depend on the approach used for dimensionality reduction/representation learning, and the simple triggering technique used for detecting events. In the following sections, we give a detailed description of the approaches we have tried, but the gist of the discussion is that a simple convolutional auto-encoder approach for representation learning and a simple auto-covariance technique for triggering result in a strong earthquake detection system, comparable in performance to the state-of-the-art *supervised* methods from the literature. The cross-dataset generalization capability of the method is quite encouraging, and its degree of success is rather insensitive to the precise details of the various architectural choices, which gives us some confidence on the soundness of the overall philosophy of the approach.

As we will discuss in our conclusion, our results open the door to further research into what precise aspects of a seismic signal our models learn to represent, and, we believe, justify the name we have given to our approach: *The seismic purifier*.

As a final note, we would like to mention that our approach is agnostic to the nature of the dataset and can be seen as a

general, unsupervised approach to time series signal detection, seismic signal detection is one example application area. Of course, this viewpoint needs to be justified by investigating the performance of the approach in other fields and data types, but due to the apparent naturality of the philosophy described above, we are cautiously optimistic that the method will indeed be useful in other fields, as well.

The code related to this work can be found at <https://github.com/onurefe/SeismicPurifier>.

II. RELATED WORK

As mentioned in the introduction, one of the prominent ways unsupervised learning appears in the seismology literature is through clustering approaches.

In Chen [2018, 2020], the authors split waveforms into segments and then apply k-means clustering to manually engineered features extracted from these segments in order to classify micro-seismic events. Duque et al. [2020] also apply various clustering algorithms (k-means clustering, BFR, CURE, BIRCH, Spectral Clustering, Expectation Maximization) to waveform segments, to classify seismic events related to Cotopaxi volcano. Huang [2019] apply hierarchical clustering in addition to k-means clustering to feature-engineered data, while Johnson et al. [2020] separate noise signals to clusters using k-means clustering on their spectral characteristics. Carniel et al. [2013] use Self-Organized Maps (SOMs) on the Fourier spectrum of waveforms recorded during phreatic events at Ruapehu volcano.

Kuyuk et al. [2011] apply SOM to engineer feature vectors to discriminate quarry blasts from earthquakes manually. Köhler et al. [2010] propose using SOM on manually engineered feature vectors for pattern classification purposes.

Along the lines of representation learning, Mousavi et al. [2019a] apply k-means clustering on feature vectors obtained using a CNN autoencoder in order to discriminate local events from teleseismic ones. Seydoux et al. [2020] use a deep scattering network to extract features and then apply Gaussian Mixture clustering to classify noise and earthquake signals.

As our summary indicates, most applications of unsupervised learning to seismology have been rather case-specific, and have not been confirmed to be efficient or stable in cross-domain applications.

III. METHODS

A. Overview of the approach

Our approach consists of the following building blocks:

- **The CNN autoencoder.** We use simple, CNN-based autoencoders with residual layers to learn a compressed representation of the waveforms. A CNN-based approach was used in order to preserve the notion of a temporal axis while preventing “mixing” between instants far from each other,¹ and to utilize the equivariance properties of CNNs under time translations.
- **Cross-covariance of representations.** Once a CNN autoencoder is trained to give an accurate reconstruction

¹Standard RNN-based approaches would also preserve time axis, but would allow such mixing.

of waveforms, the bottleneck layer of the autoencoder can be thought to give a compressed, efficient representation of the information content of the waveform. Motivated by the intuition that the arrival of a real signal should be represented as strong temporal changes in this information-rich representation, we compute the cross-covariance of such compressed representations (along the time direction). If the cross-covariance of two related (to be made precise below) representations have a well-defined, prominent peak at $\Delta t = 0$, we expect the waveform to contain an actual signal. If there is no such prominent peak, there should be no significant, temporally localized change in the signal and we expect the waveform to represent pure noise.

We try various choices for the pairs of representations used in this cross-covariance computation and for combining multiple covariances into a single overall cross-covariance profile. We observe that the results are insensitive to the choices tried. Even a simple auto-covariance followed by averaging over channels, as described below, gives good results.

- **Triggering.** Finally, to make the signal/no signal decision based on the overall cross-covariance profile obtained in the previous step, we need to use a triggering method. We tried a few choices such as looking at the maximum value or using a simple weighted average, and observed that the results are rather insensitive to this choice, as well.

Below, we describe each one of these building blocks and the choices tried for them in detail.

B. The CNN autoencoder

1) *The loss:* The aim of an autoencoder is to reconstruct the input by using a compressed representation. Thus, the loss function should measure how similar the output is to the input. We use a simple root-mean-squared loss on centered versions of the input and the output. In other words, if $x \in \mathbb{R}^{N \times C}$, $y \in \mathbb{R}^{N \times C}$ denote the input and output of the model with N and C being the number of timesteps and channels of the input waveforms² we center each input/output channel to get $\frac{1}{N} \sum_{n=0}^{N-1} x_{nc} = 0$, $\frac{1}{N} \sum_{n=0}^{N-1} y_{nc} = 0$ where $n \in [0, N - 1]$ and $c \in [0, C - 1]$, and use the reconstruction loss

$$L_{recons} = \sqrt{\frac{1}{NC} \sum_{n=0}^{C-1} \sum_{n=0}^{N-1} (x_{nc} - y_{nc})^2} \quad (1)$$

2) *Building blocks:* Our CNN autoencoders consist of three main building blocks that we call Downsampling, Residual, and Upsampling layers. The Downsampling and Residual layers together form the encoder part of the model, and the Upsampling layers form the decoder. A visual representation can be found in Figures 2 and 1.

a) *Downsampling layers:* The Downsampling layers consist of a reflective padding, followed by a 1-dimensional convolution with stride 2 and batch normalization, and have ReLU activation. Due to the stride, the output length of a

Downsampling layer along the time direction is half its input length.

Five Downsampling layers with convolutional window sizes 15, 13, 11, 9, 7 and output channel (filter) counts 8, 16, 32, 64, 64 are used in succession, which reduces the length of input waveforms along the time axis from 3000 to 94 while increasing the number of channels from 3 to 64.

Since some of the output lengths are not divisible by 2, we use a separate “reflect padding” layer to make the lengths compatible between Downsampling layers.

b) *Residual layer:* The Downsampling layers are followed by a series of “Residual” layers. These layers do not change the dimensions of their input, but aim to further strengthen the representation being learned by utilizing two identical stacks containing 1D Convolution, Batch Normalization, and ReLU Activation layers. We add and a residual (“skip”) connection around these stacks that adds the input to the Residual layer to the output of the second stack, as shown in 1c. This sum is then passed through a ReLU activation to form the output.

We use five of these Residual layers with 64 filter and filter window size 5. The last Residual layer uses linear activation instead of ReLU.

c) *Upsampling layer:* Finally, the output of the series of Residual layers is connected to a series of Upsampling layers that form the decoder. These layers consist of plain upsampling followed by padding, 1-dimensional convolution, batch normalization and and a ReLU activation.

Five such upsampling layers with convolutional window sizes 7, 9, 11, 13, 15 and filter counts 32, 16, 8, 4, and 3 are used to increase the length of the waveform representations along the time axis from 94 to 3000 while decreasing the number of channels from 64 to 3.

Dually to the Downsampling case, each Upsampling layer doubles the temporal length of its output. Once again, to ensure shape compatibility of the final decoded output with the original waveform input, we use a cropping layer. See Figure 2 for a visual representation.

3) *Denoising autoencoder:* Our experiments show that by injecting noise into the input of the autoencoder and training the autoencoder to eliminate the noise at the output, we can improve the filtering properties and generalization performance. Autoencoders trained this way are called denoising autoencoders.

Specifically, in this approach, we add Gaussian noise with zero mean and $\sigma = 0.2$ to the input normalized to $\sigma = 1$ for each channel. The reconstruction loss 1 is then computed between the model output and the input signal.

We use this denoising approach in the “Autocovariance” and “Augmentation Cross-covariance” methods described below.³

C. The cross-covariance layer

The cross-covariance layer is a custom layer that calculates the cross-covariance of two latent representations efficiently by taking advantage of Fast Fourier Transform (FFT). Cross-covariance is calculated between channels of the two representations individually and then averaged over all channels. After

²Which happen to be (3000, 3), respectively, as we describe in our section on data preparation

³For the “Representation cross-covariance” method, we use a simple autoencoder with no denoising.

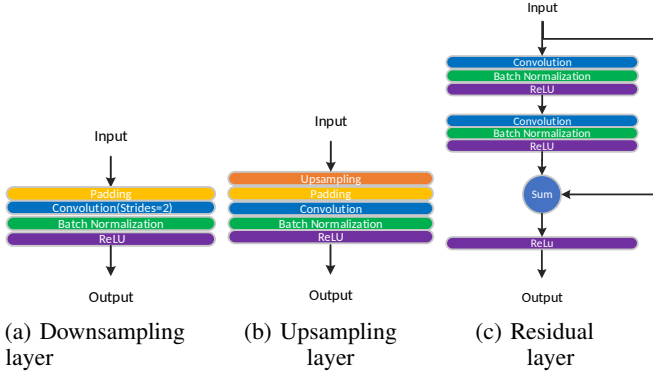


Fig. 1: Building blocks

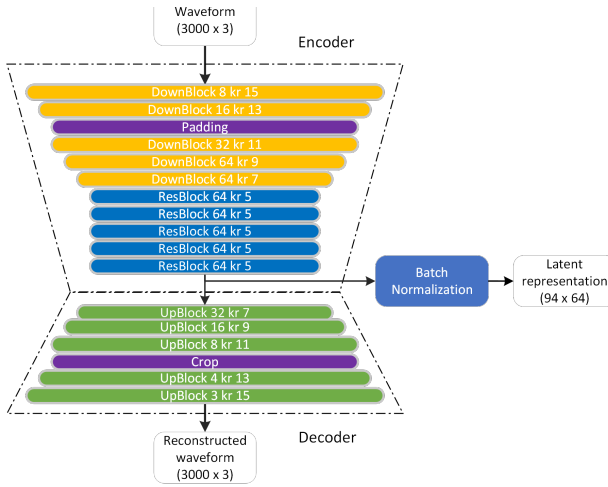


Fig. 2: CNN autoencoder

describing the general cross-covariance computation, we give a discussion of the choices for the representation pairs whose covariances we tried in our detection procedure.

Let $g \in \mathbb{R}^{N_L \times C_L}$, $h \in \mathbb{R}^{N_L \times C_L}$ represent two latent representations where N_L and C_L denote the number of timesteps and channels of the latent space, respectively. We first center both representations such that the mean of each channel is zero ($\frac{1}{N_L} \sum_n g_{nc} = 0$, $\frac{1}{N_L} \sum_n h_{nc} = 0$). We do not strictly normalize the representations since amplitude information is important for detection. However, we apply a Batch Normalization layer to both representations before computing the cross-covariances (see Figure 2, the Batch Normalization layer).

The n th entry c_n of the cross-covariance of two representations g and h is given by

$$c_n = \frac{1}{C_L} \sum_{c=0}^{C_L-1} \left[\frac{1}{N_L} \sum_{n'=0}^{N_L-1} g_{n',c} h_{n'+n,c} \right] \quad (2)$$

where $n \in [-\frac{N_L}{2}, \frac{N_L}{2} - 1]$. Due to efficiency considerations, cross-covariances are calculated by circular convolutions, which is equivalent to calculating covariance for periodic g_{nc} and

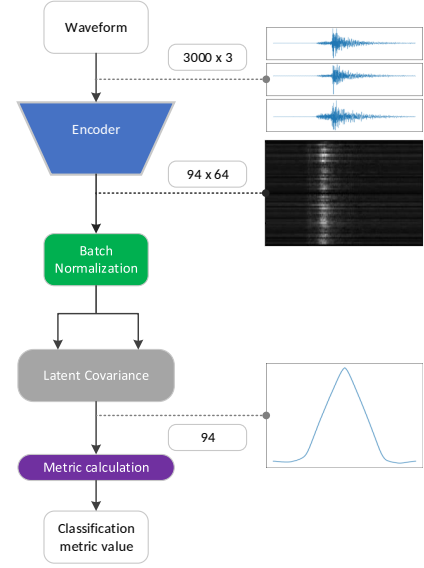


Fig. 3: Autocovariance method diagram

h_{nc} ⁴

With the periodicity assumption, the cross-covariance of two representations can be computed by computing the inverse FFT of the product of the per-channel FFTs of the two representations.

D. Pair choices for cross-covariance

As mentioned above, we have experimented with different pairs of inputs to the cross-covariance calculation, which we describe below.

a) *Autocovariance.*: The simplest approach to using the cross-covariance between two signals is to use the same representation for both inputs, in other words, to use the autocovariance of each channel (averaged over all channels). We observe that contrary to noise waveforms, earthquake representations obtained by training an autoencoder tend to be composed of more long-term features—while the autocovariance of noise samples results in a narrow spike at $\tau = 0$, for earthquake signals, we obtain a wider and smoother peak. This is in line with the intuitive motivation described above, and allows one to use very simple triggering criteria measuring the prominence of the peak observed in autocovariance.

b) *Augmentation cross-covariances.*: Another method involves applying random augmentations to raw waveforms and then taking the cross-covariances of their latent representations obtained by using the same autoencoders on each. The method has similarities to Self-Supervised Learning (SSL) Liu et al. [2021], which uses augmentations to obtain robust representations for classification purposes.

The intuitive motivation for this approach is that earthquake waveforms are expected to be composed of robust features, so small changes in the raw waveform shouldn't significantly alter

⁴I.e., $g_{nc} = g_{n+N_L,c}$ and $h_{nc} = h_{n+N_L,c}$. It is possible to use, e.g., zero padding instead of circular convolutions, however, our experiments have shown that this doesn't improve the performance while increasing the computational cost.

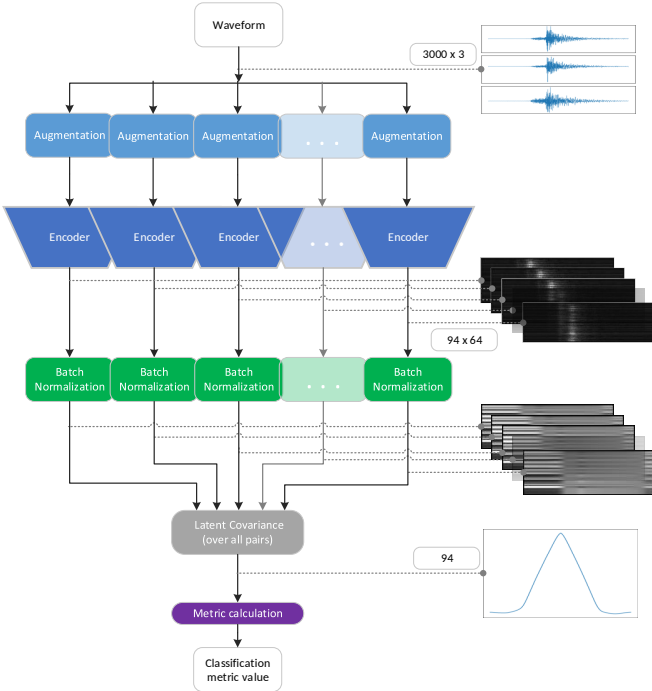


Fig. 4: Augmentation Cross-covariances method diagram

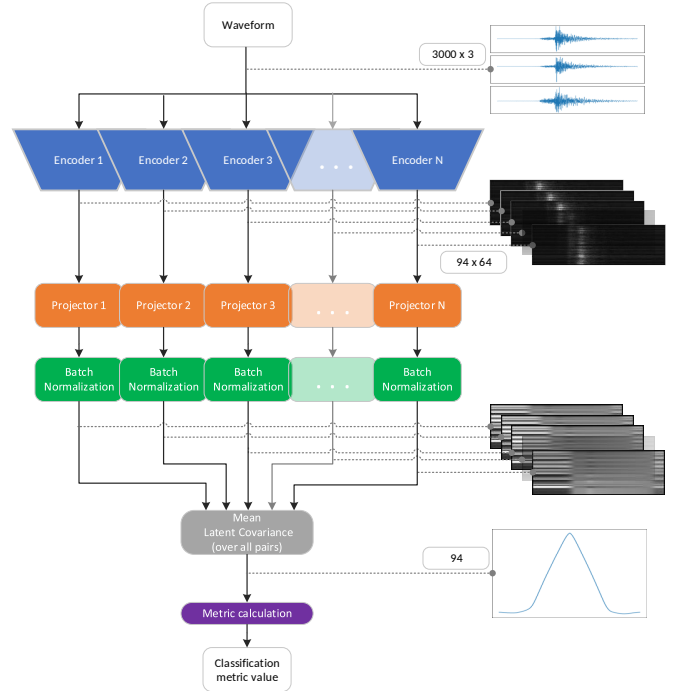


Fig. 5: Representation Cross-covariances method diagram

their latent representations. As a result, the cross-covariance of the latent representations of two augmented waveforms is expected to give a more robust peak than what gets for a noise waveform and its augmentations.

We have observed that using an ensemble of augmentations and computing the average of the pairwise cross-covariances (instead of just using two augmentations) improves stability and performance.

As for the specific augmentation technique to use, we tried some of the standard time series data augmentation techniques Wen et al. [2020] such as simple additive noise and phase warping (adding random phase in the frequency domain), and our experiments have shown that time warping augmentation performs well and gives more stable results compared to other methods.

Time warping is accomplished by remapping the time axis of the original waveform by a monotonically increasing function. The relevant function is obtained by selecting random deviations from the actual time at certain “knots”, and interpolating between the knots with the BSpline algorithm and discretizing. We sample 4 knots from a zero-mean Gaussian distribution with standard deviation 0.15.

c) Representation cross-covariances.: This method involves using an ensemble of encoder-decoder structures to obtain multiple waveforms representations from a single waveform. The idea is similar to the augmentation-based method in that once the autoencoders are trained, we compute the average of the pairwise cross-covariances of different autoencoders (instead of different augmentations).

One important point is that this approach affects the training phase as well: Since a multitude of autoencoders can learn completely different representations, computing the pairwise covariances of otherwise unconstrained autoencoders may not

be an effective way to detect signals. To make the outputs of the autoencoders comparable, we also learn an additional set of linear “projection” matrices at the output of each autoencoder.⁵ These matrices are trained to maximize the similarities between the corresponding channels of different autoencoders.

More explicitly, we simultaneously train the projection matrices and the autoencoders, but as before, the gradient updates of the autoencoders only use the reconstruction loss to allow different autoencoders to learn different representations, while the gradient updates for the projection matrices use another RMS loss as described below, to map the outputs of different autoencoders to each other.

Let $h^e \in \mathbb{R}^{N_L \times C_L}$ denote projected latent representation of the e 'th member of the ensemble where N_L and C_L are latent numbers of timesteps and channels, respectively. Before calculating the loss for training the projection matrices, each channel $c \in [0, C_L - 1]$ is centered to $\sum_n h_{nc}^e = 0$ and normalized to unit variance. The projection loss L_{proj} is then calculated as the RMS difference between pairs of projected representations, the mean being taken over all pairs, channels, and time steps.

We emphasize that the gradient updates of the projection matrices and the autoencoder layers are made with respect to different losses, in order to allow the system to learn different representations while also learning to relate them to each other. As we report below, the representation cross-covariances method described here outperforms the others we tried by a small margin and is more robust.

⁵In line with common usage in the ML literature, we use the word “projection” for a linear map that transforms features instead of following the mathematical definition as an idempotent linear operator.

E. Triggering: classification metrics

In line with the motivating intuition described in the introduction, our observations show that the covariance profiles obtained from latent representations have a wider and smoother peak for earthquake samples, whereas one gets a narrow (and shallow) spike at $\tau = 0$ for noise samples.

Thus, any reasonable metric measuring the overall prominence of the peak in auto/cross-covariance profile should provide a good classification score without the need for supervised training.

We tried a variety of such metrics and they all gave similarly good results. The simplest such metric is the height of the peak in autocovariance; here we report our results on a metric that consists of a weighted average of the autocovariance along the time direction, with the weights being given by a Gaussian with a center at $\tau = 0.0$ seconds and a width of $\sigma_0 = 5.0$ seconds. Our results were not sensitive to the choice of this width.

More explicitly, if c_n denotes the auto/cross-covariance at the discrete time n , the detection metric M is given by

$$M = \frac{1}{\sqrt{2\pi\sigma_0^2}} \sum_n \exp\left(-\frac{t_n^2}{2\sigma_0^2}\right) c_n \Delta t \quad (3)$$

where Δt is the timestep size of the latent representation.

By choosing a threshold on this metric (which is analogous to the output score of a supervised model), we will be able to change the true positive and false positive rates of the detection system, and evaluate the detection performance via the threshold-independent score of ROC-AUC.

IV. TRAINING AND TESTING PROCEDURES

A. Datasets and preprocessing

We used two different datasets in order to be able to evaluate the cross-domain performance of the models. The datasets STEAD Mousavi et al. [2019b] and INSTANCE Michellini et al. [2021] were selected since they are prepared in a way that facilitates a meaningful evaluation of models trained on each other, are obtained from different regions, and use different limits on epicenter distance, making them suitable for cross-domain evaluation. The properties of both datasets are summarized in Table IV-A.

Dataset	STEAD	INSTANCE
Channels	E, N, Z	E, N, Z
Earthquake waveforms	1,050,000	1,159,249
Noise waveforms	100,000	132,330
Sampling Rate	100Hz	100Hz
Time Window	60s	120s
Epicenter Distance	< 350km	< 600km
Region	Global	Italy

TABLE I: Properties of the STEAD and INSTANCE datasets.

We aimed to make our evaluation procedures compatible with the review article Münchmeyer et al. [2022] where a range of models have been compared on various datasets. For this purpose, we chose the model input time window to be 30 seconds, applied bandpass filtering (1 – 20Hz) and normalized the waveforms along the time axis to make the standard deviation of each channel equal to 1.

To form the training set, we followed the procedure described in Münchmeyer et al. [2022], Woollam et al. [2022] to randomly crop 2/3 of the earthquake waveforms in a way that guarantees to have at least one phase arrival within the window, and randomly cropped the remaining earthquake waveforms and all of the noise waveforms without any such constraint.

In the testing phase, following Münchmeyer et al. [2022], Woollam et al. [2022], we cropped the the earthquake waveforms in a way that guarantees that the onset time is inside the window with a 3-second margin.

As in Münchmeyer et al. [2022], we used 60% of the whole data set for training, however, to get a more robust measure of test performance, we used 5-fold cross validation at the test phase instead of using a single hold-out. Thus, instead of the 10% validation and 30% test size used in Münchmeyer et al. [2022], Woollam et al. [2022], we used 20% for both.

B. Training

We used 5-fold cross-validation to train and evaluate 5 models on both STEAD and INSTANCE datasets, and trained the models for 20 epochs with a batch size of 256 samples. We selected the epoch with the lowest validation error.

We used the ADAM optimizer with a learning rate of 10^{-4} and $\epsilon = 10^{-7}$, although higher learning rate values were also seen to give stable results. Moment estimating moving average filter coefficients β_1 and β_2 were chosen to be 0.99 and 0.999, respectively. We kept other settings in their default values, in particular, we use additional exponential moving average filtering, weight decay, or gradient clipping.

Our training was done on a workstation with a single NVIDIA GTX3090TI GPU. Training the CNN autoencoder took 1.5 minutes per epoch on the INSTANCE dataset and 1.25 minutes on the STEAD dataset. For the “ensemble of autoencoders” method, per-epoch training times were 7.5 minutes for INSTANCE and 6.5 minutes for STEAD. Since we used preprocessed data, a negligible amount of time was spent on data generation.

Since the datasets (especially STEAD) involve waveforms with gaps, we obtain unnatural waveforms related to quantization noise for some samples after the cropping operation. This effect degrades the performance of the proposed models. To tackle this problem, we injected a tiny amount of noise (with a standard deviation of 10^{-6}) into all cropped waveforms.

C. Testing

Our tests have been conducted similarly to the review article Münchmeyer et al. [2022], except, as mentioned above, we used a 5-fold cross-validation for each dataset.

As in Münchmeyer et al. [2022], we discard test examples that don’t include an onset time margin of 3 seconds. As in the training case, we inject a tiny amount of noise (with a standard deviation of 10^{-6}) into the cropped waveforms.

We used the same metric for the evaluation as Münchmeyer et al. [2022], namely, the Area Under the Receiver Operating Characteristic curve (ROC-AUC). This is obtained by plotting the True Positive Rate (TPR) against the False Positive Rate (FPR) as one varies the threshold value used for triggering.

	INSTANCE (Testing)	STEAD (Testing)		
INSTANCE (Training)	Autocovariance	0.964 ± 0.012	Autocovariance	0.974 ± 0.009
	Autocovariance (Denoising)	0.972 ± 0.002	Autocovariance (Denoising)	0.985 ± 0.001
	Augmentation	0.970 ± 0.005	Augmentation	0.985 ± 0.004
	Cross-covariances		Cross-covariances	
	Augmentation	0.972 ± 0.002	Augmentation	0.987 ± 0.001
	Cross-covariances (Denoising)		Cross-covariances (Denoising)	
	Representation	0.976 ± 0.001	Representation	0.988 ± 0.001
	Cross-covariances		Cross-covariances	
	Phasenet	0.964	Phasenet	0.994
	EQTransformer	0.957	EQTransformer	0.990
STEAD (Training)	Autocovariance	0.973 ± 0.001	Autocovariance	0.985 ± 0.001
	Autocovariance (Denoising)	0.972 ± 0.004	Autocovariance (Denoising)	0.985 ± 0.004
	Augmentation	0.973 ± 0.001	Augmentation	0.987 ± 0.001
	Cross-covariances		Cross-covariances	
	Augmentation	0.972 ± 0.002	Augmentation	0.987 ± 0.002
	Cross-covariances (Denoising)		Cross-covariances (Denoising)	
	Representation	0.974 ± 0.001	Representation	0.988 ± 0.001
	Cross-covariances		Cross-covariances	
	Phasenet	0.941	Phasenet	1.000
	EQTransformer	0.966	EQTransformer	1.000

TABLE II: Method ROC-AUC scores for different training (rows) and testing (columns) datasets. Phasenet and EQTransformer performances are taken from the article Münchmeyer et al. [2022]

As opposed to single-threshold metrics such as accuracy, ROC-AUC measures the global performance of a model by evaluating its scoring system as a whole, and thus is a more robust measure of the model performance.⁶

V. RESULTS

Our final results are summarized in Table IV-B, which includes performance results from separate cross-validation runs on STEAD and INSTANCE, and also cross-dataset performance obtained by training on one dataset and testing on the other.

When we look at the same-dataset (cross-validation) performance, we see that our proposed methods outperform their supervised counterparts on the INSTANCE dataset by a non-negligible margin, while the supervised methods perform better on the STEAD dataset.

Looking at the cross-dataset performance, we see that our methods give better results than supervised methods for training on STEAD and testing on INSTANCE, while supervised methods win for training on INSTANCE and testing on STEAD.

One striking aspect of our results is the small change in performance when one changes datasets. For instance, for a given training set, same-dataset test performance and cross-dataset test performance (i.e., results in the same row of the 2×2 result matrix in Table IV-B) are much closer to each other than what is seen with the supervised methods. In other words, the cross-validation score (AUC) one sees in one dataset is more representative of what one gets for using the model on the other dataset. For instance, when a model is trained on the INSTANCE dataset, the performance of the Representation Cross-covariances method changes by 0.012 when one changes the test set, whereas for Phasenet the change is 0.030, and for EQTransformer it is 0.033. For

training on STEAD, the changes in performance between test sets are 0.012 for Representation Cross-covariances, 0.059 for Phasenet, and 0.034 for EQTransformer.

Similarly, for a given test set, the results of our methods have less dependence on the training set used (i.e., results in the same column of Table IV-B are close to each other for our methods). For instance, for testing the Representation Cross-covariances method on INSTANCE, there is a 0.002 difference between the AUC scores obtained by using two different training sets, whereas for Phasenet Zhu and Beroza [2019] there is a difference of 0.023, and for EQTransformer, there is a difference of 0.009. Similarly, for testing the Representation Cross-covariances method on STEAD, there is no appreciable difference between the scores for different training sets at the uncertainty level of 0.001, whereas Phasenet gives a difference of 0.006 and EQTransformer gives a difference of 0.010. We find this stability of results rather encouraging.

Finally, let us note that our experiments have shown that without the “tiny noise injection” described previously, only the Representation Cross-covariances method has a performance similar to those of the best supervised methods. However, by injecting noise, we see that all our proposed methods become comparable to supervised methods in terms of ROC-AUC score.

VI. EXAMPLES OF LATENT REPRESENTATIONS

Given that a simple way of quantifying the information in the latent representations gives a strong detection system, one immediately wonders what exactly these representations encode. By inspecting the feature “excitations” in the bottleneck, can we say something about the nature of the earthquake (or noise) the model is representing? Could the features themselves be valuable source of information beyond the use of a simple triggering for event detection?

⁶Except in settings with extreme class imbalance.

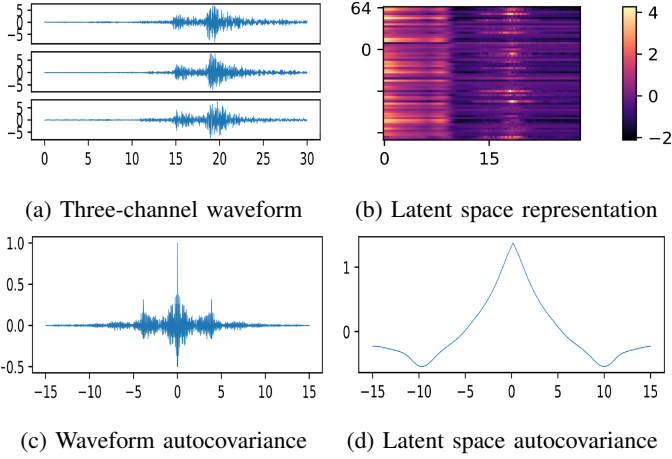


Fig. 6: Autoencoder earthquake waveform sample

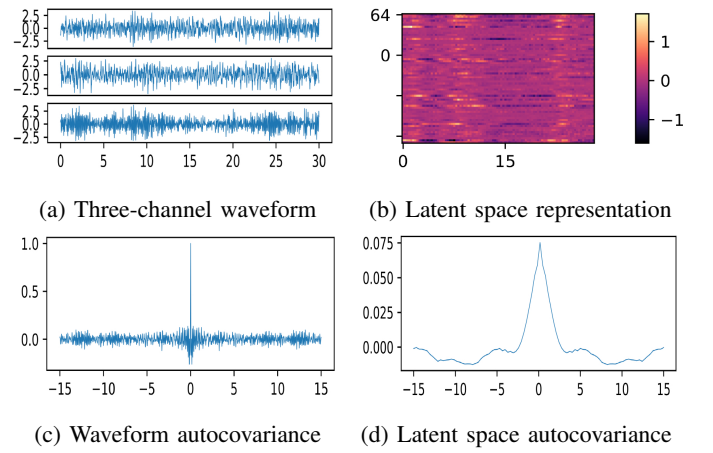


Fig. 7: Autoencoder noise waveform sample

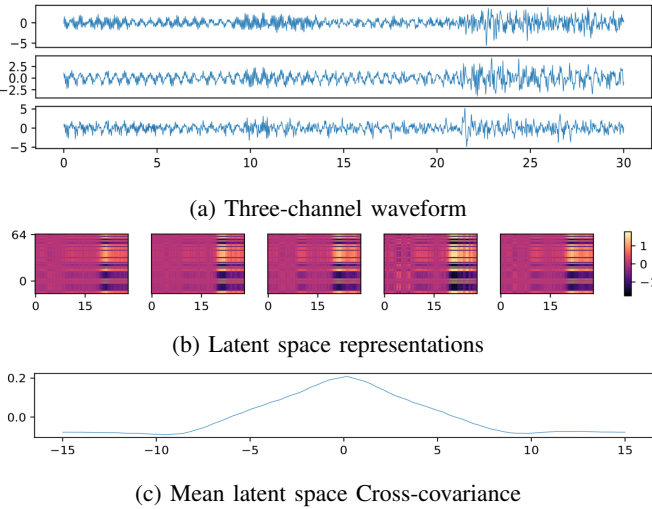


Fig. 8: Representation cross-covariances method earthquake waveform sample

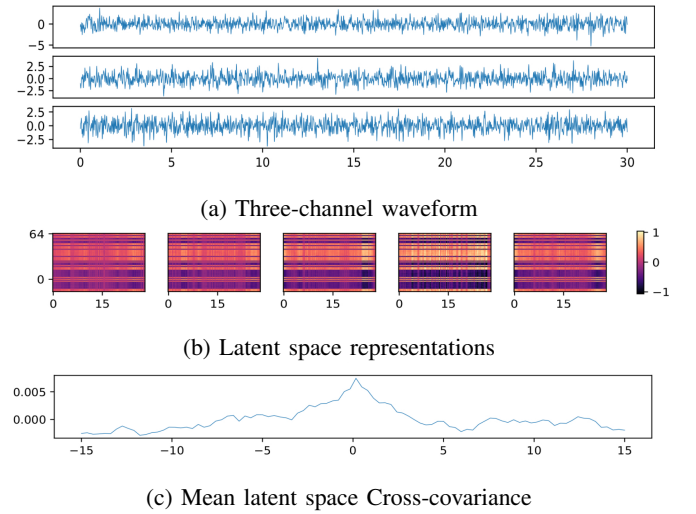


Fig. 9: Representation cross-covariances method noise waveform sample

In this section, we show some representative plots to have an initial look at what the latent representations look like for different kinds of waveforms. In the supplementary sections, we give further examples. We believe a thorough investigation of the latent representations may prove beneficial.

In addition to latent representations, we also show cross/auto-covariance profiles obtained from these representations used in the triggering/detection procedure.

In Figures 6, 7, we show the latent space representations obtained by the autoencoder model trained for the *autocovariance* approach for an earthquake and a noise waveform. We see that the activations for the earthquake signal have a clear “phase transformation” in time, whereas those of the noise waveform do not. Relatedly, the autocovariance profile obtained from the representations is much more prominent for the earthquake waveform compared to that of the noise waveform.

Similarly, in Figures 8 and 9, we show the “projected” representations of different encoders trained for the *Representation cross-covariances* approach. Since we train the linear

projectors mapping different sets of representations to each other using similarity loss, these projections emphasize the common parts of the different representation sets. We see that in the earthquake sample, there is once again a very strong “phase transformation” in time, with time intervals with significant seismic activity getting coded in a clear way, resulting in a more prominent covariance profile for the earthquake compared to the noise waveform.

Further samples can be found in the supporting documents section A.

VII. DISCUSSION AND FUTURE WORK

Our experiments show that the unsupervised methods described have comparable detection performance to supervised methods trained specifically for the detection task, in some cases surpassing them. In addition, the performance of the proposed methods varies little when different datasets are used for training and testing, which suggests that they are less prone to overfitting and have good generalization properties.

Although we applied them to the seismic waveform classification task, our methods have the potential to be domain-agnostic and can be tried on other multidimensional time series data for discriminating background noise from meaningful signals. We are planning to investigate their performance in a range of signal detection tasks to their potential as a “Swiss Army knife” for time series signal detection.

Although our methods form candidate solutions to the signal detection problem, in their current state, they can’t detect the signal arrival times, in other words, they can’t be used for accurate phase picking. Another further avenue of research involves developing unsupervised methods that can also perform accurate phase picking. The Representation cross-covariances method seems to provide cleanly segmented representations for earthquakes, which can be a good starting point for developing unsupervised phase picking.

Various checks have indicated that our models tend to be less prone to false negatives than false positives. Further investigation and spot-checks of a range of examples have indicated that false positives most often occur when the methods are wrongly triggered for cases where there is, e.g., an instrumental glitch in a noise sample which makes it appear like an actual signal, but they are much less prone to missing real signals of small magnitude. This suggests that there is a chance to further improve the performance by combining it with other approaches to deal with these exceptional cases.

Additional research directions motivated by our approach include utilizing this framework for multi-station signal detection, systematic deep dives into the latent representations to characterize the precise aspects of signals the models are learning to represent, and to apply to method to continuous time series.

There is a range of directions to explore and many possibilities for further experimentation and improvements for the proposed approach. We hope these explorations will open the door to new applications of machine learning to seismology.

VIII. ACKNOWLEDGEMENTS

We would like to thank Dr. Yaman Özakın, Dr. Ali Özgün Konca, Dr. Hayrullah Karabulut, and Dr. Birsen Can for helpful discussions and guidance. We are grateful for the contributions of the EarthML research group’s former members in building this study’s foundations. This research has been supported by the Turkish Scientific and Technical Research Council (TÜBİTAK) with grant number 118C213 under the BİDEB 2232 program.

© 20xx IEEE. Personal use of this material is permitted. Permission from IEEE must be obtained for all other uses, in any current or future media, including reprinting/republishing this material for advertising or promotional purposes, creating new collective works, for resale or redistribution to servers or lists, or reuse of any copyrighted component of this work in other works.

REFERENCES

- S Mostafa Mousavi, William L Ellsworth, Weiqiang Zhu, Lindsay Y Chuang, and Gregory C Beroza. Earthquake transformer—an attentive deep-learning model for simultaneous earthquake detection and phase picking. *Nature communications*, 11(1):3952–3963, 2020.
- Hugo Soto and Bernd Schurr. Deepphasepick: a method for detecting and picking seismic phases from local earthquakes based on highly optimized convolutional and recurrent deep neural networks. *Geophysical Journal International*, 227(2): 1268–1294, 2021.
- Jack Woollam, Andreas Rietbrock, Angel Bueno, and Silvio De Angelis. Convolutional neural network for seismic phase classification, performance demonstration over a local seismic network. *Seismological Research Letters*, 90(2A): 491–502, 2019.
- Weiqiang Zhu and Gregory C Beroza. Phasenet: a deep-neural-network-based seismic arrival-time picking method. *Geophysical Journal International*, 216(1):261–273, 2019.
- Zachary E. Ross, Men-Andrin Meier, Egill Hauksson, and Thomas H. Heaton. Generalized seismic phase detection with deep learning. *Bulletin of the Seismological Society of America*, 108(5A):2894–2901, 2018.
- Jannes Münchmeyer, Jack Woollam, Andreas Rietbrock, Frederik Tilmann, Dietrich Lange, Thomas Bornstein, Tobias Diehl, Carlo Giunchi, Florian Haslinger, Dario Jozinović, Alberto Michelini, Joachim Saul, and Hugo Soto. x". *Journal of Geophysical Research: Solid Earth*, 127(1): e2021JB023499, 2022.
- Yangkang Chen. Fast waveform detection for microseismic imaging using unsupervised machine learning. *Geophysical Journal International*, 215(2):1185–1199, 2018.
- Yangkang Chen. Automatic microseismic event picking via unsupervised machine learning. *Geophysical Journal International*, 222(3):1750–1764, 2020.
- Adrian Duque, Kevin Gonzalez, Noel Perez, Diego Benitez, Felipe Grijalva, Roman Lara-Cueva, and Mario Ruiz. Exploring the unsupervised classification of seismic events of cotopaxi volcano. *Journal of Volcanology and Geothermal Research*, 403:107009, 2020.
- Weilin Huang. Seismic signal recognition by unsupervised machine learning. *Geophysical Journal International*, 219(2):1163–1180, 2019.
- Christopher W Johnson, Yehuda Ben-Zion, Haoran Meng, and Frank Vernon. Identifying different classes of seismic noise signals using unsupervised learning. *Geophysical Research Letters*, 47(15):e2020GL088353, 2020.
- Roberto Carniel, Arthur D Jolly, and Luca Barbui. Analysis of phreatic events at ruapehu volcano, new zealand using a new som approach. *Journal of volcanology and geothermal research*, 254:69–79, 2013.
- HS Kuyuk, E Yildirim, E Dogan, and G Horasan. An unsupervised learning algorithm: application to the discrimination of seismic events and quarry blasts in the vicinity of istanbul. *Natural Hazards and Earth System Sciences*, 11(1):93–100, 2011.
- Andreas Köhler, Matthias Ohrnberger, and Frank Scherbaum. Unsupervised pattern recognition in continuous seismic wavefield records using self-organizing maps. *Geophysical Journal International*, 182(3):1619–1630, 2010.
- S Mostafa Mousavi, Weiqiang Zhu, William Ellsworth, and Gregory Beroza. Unsupervised clustering of seismic signals using deep convolutional autoencoders. *IEEE Geoscience and Remote Sensing Letters*, 16(11):1693–1697, 2019a.
- Léonard Seydoux, Randall Balestriero, Piero Poli, Maarten de Hoop, Michel Campillo, and Richard Baraniuk. Clustering earthquake signals and background noises in continuous seismic data with unsupervised deep learning. *Nature communications*, 11(1):3972–3983, 2020.
- Xiao Liu, Fanjin Zhang, Zhenyu Hou, Li Mian, Zhaoyu Wang, Jing Zhang, and Jie Tang. Self-supervised learning: Generative or contrastive. *IEEE transactions on knowledge and data engineering*, 35(1):857–876, 2021.
- Qingsong Wen, Liang Sun, Fan Yang, Xiaomin Song, Jingkun Gao, Xue Wang, and Huan Xu. Time series data augmentation for deep learning: A survey. *arXiv preprint arXiv:2002.12478*, 2020.
- Seyed Mostafa Mousavi, Yixiao Sheng, Weiqiang Zhu, and Gregory C Beroza. Stanford earthquake dataset (stead): A global data set of seismic signals for ai. *IEEE Access*, 7: 179464–179476, 2019b.
- Alberto Michelini, Spina Cianetti, Sonja Gaviano, Carlo Giunchi, Dario Jozinović, and Valentino Lauciani. Instance—the italian seismic dataset for machine learning. *Earth System Science Data*, 13(12):5509–5544, 2021.
- Jack Woollam, Jannes Münchmeyer, Frederik Tilmann, Andreas Rietbrock, Dietrich Lange, Thomas Bornstein, Tobias Diehl, Carlo Giunchi, Florian Haslinger, Dario Jozinović, Alberto Michelini, Joachim Saul, and Hugo Soto. Seisbench—a toolbox for machine learning in seismology. *Seismological Research Letters*, 93(3):1695–1709, 2022.

APPENDIX A LATENT SPACE SAMPLES

In Figures 1-10 we give further examples of latent space (“bottleneck”) representations of various noise and earthquake waveforms obtained by using a CNN autoencoder or an ensemble of CNN autoencoders with projection heads (without injecting noise), and the resulting covariance profiles. We both give examples where the method behaves “appropriately” (giving a strong covariance profile for earthquakes and a weak one for noise), and some typical examples where it is “misled”. The special characteristics of the latter cases shed some light into the failure modes of the method.

APPENDIX B

THE EFFECT OF TRAINING DURATION ON PERFORMANCE

During the training of our models, we avoided informing the model or the tuning procedures about the performance of the final detection method—our aim was to have a purely unsupervised model, unaware of the final detection task in any way. In particular, the choice of epoch was made by using purely the unsupervised metrics, and the detection system was created for the best models for the unsupervised problem.

However, it is interesting to inspect the detection performance of the model at different epochs to see the behavior of the system as the training progresses, and to get some insight into the robustness of the method. For this purpose, we created detection systems using models at different epochs during the unsupervised training, and evaluated their detection performance. In Figure 11, we show the ROC-AUC scores of various methods as a function of the epoch number. Cross-validation (CV) allows us to show both the mean AUC at each epoch over the CV folds, and the min and max values over the folds.

We see that the Representation cross-covariances method has better stability over the training duration than the other methods. Its best AUC score is better than those of the others by a small margin, and its scores deviate less from split to split.

The Augmentation cross-covariances method also gives decent performance and is rather stable over epochs, suggesting that ensemble methods could have stability and performance advantages. Augmentation cross-covariances and Autocovariance methods have close performances at their best versions, while the Representation Cross-covariances method is better by a small margin for all domains. The Autocovariance method is the most sensitive to training duration among all.

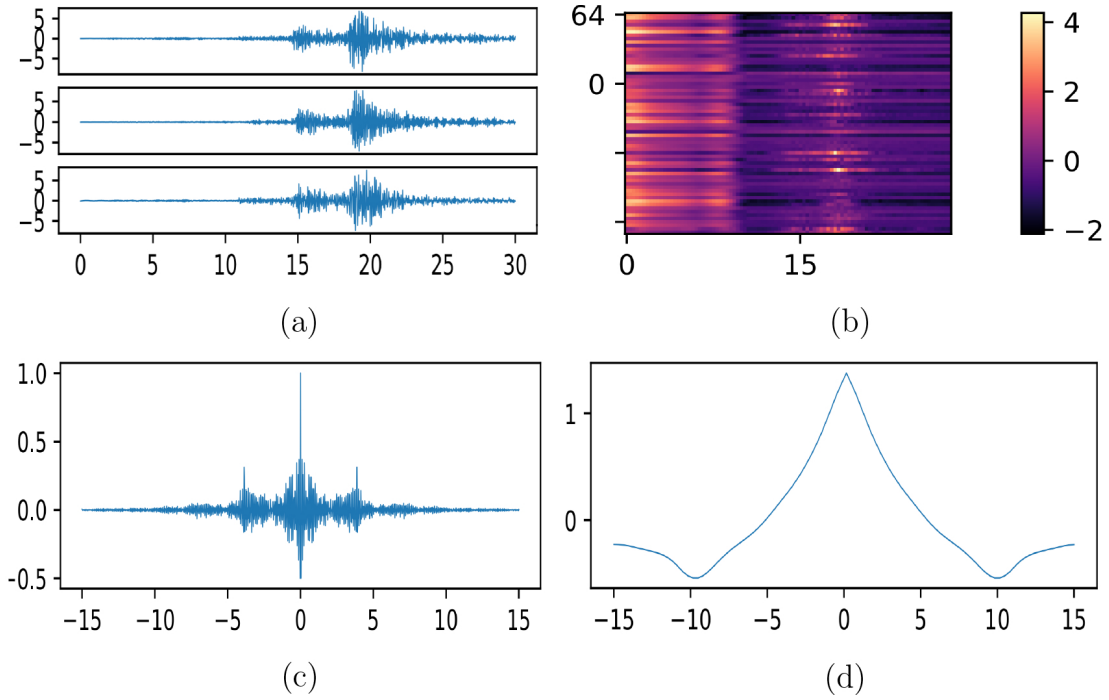


Fig. 1: Autoencoder earthquake sample 1 (a) three-channel waveform, (b) latent space representation, (c) waveform Autocovariance, (d) latent space Autocovariance. The x -axis in the representation plot is “compressed time”, the y -axis is the channel index, and the color coding represents the activation level of the relevant channel at the given instance. Note the strong covariance profile and the temporal “phase transitions” in the latent space representations.

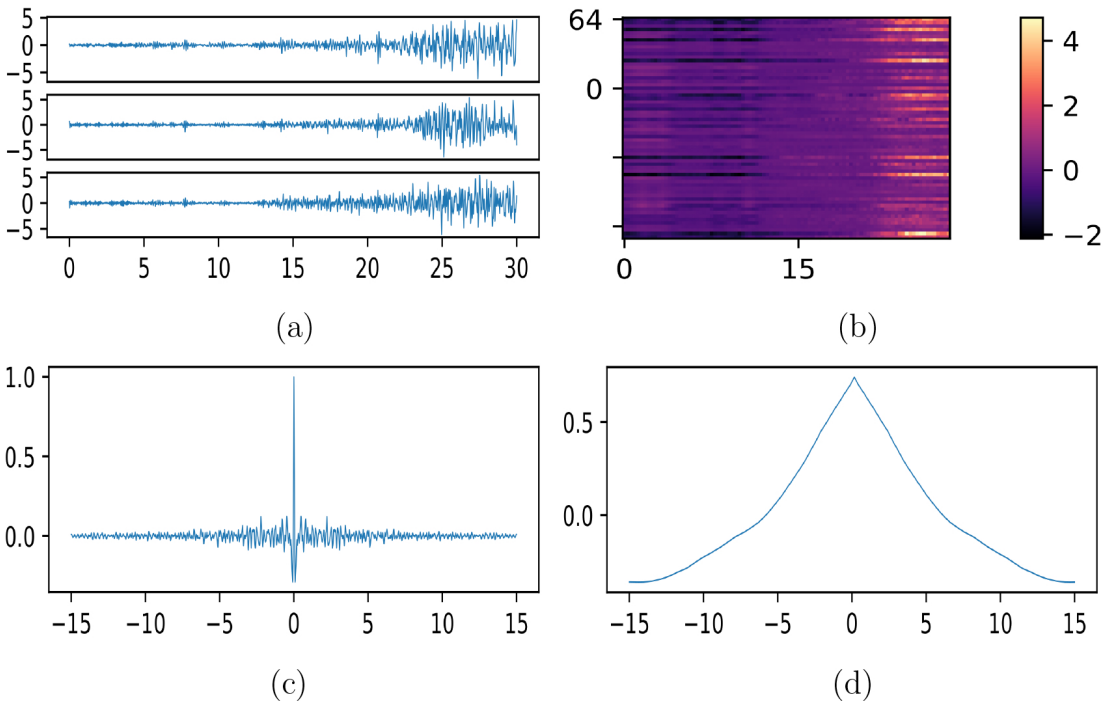


Fig. 2: Autoencoder earthquake sample 2 (a) three-channel waveform, (b) latent space representation, (c) waveform Autocovariance, (d) latent space Autocovariance.

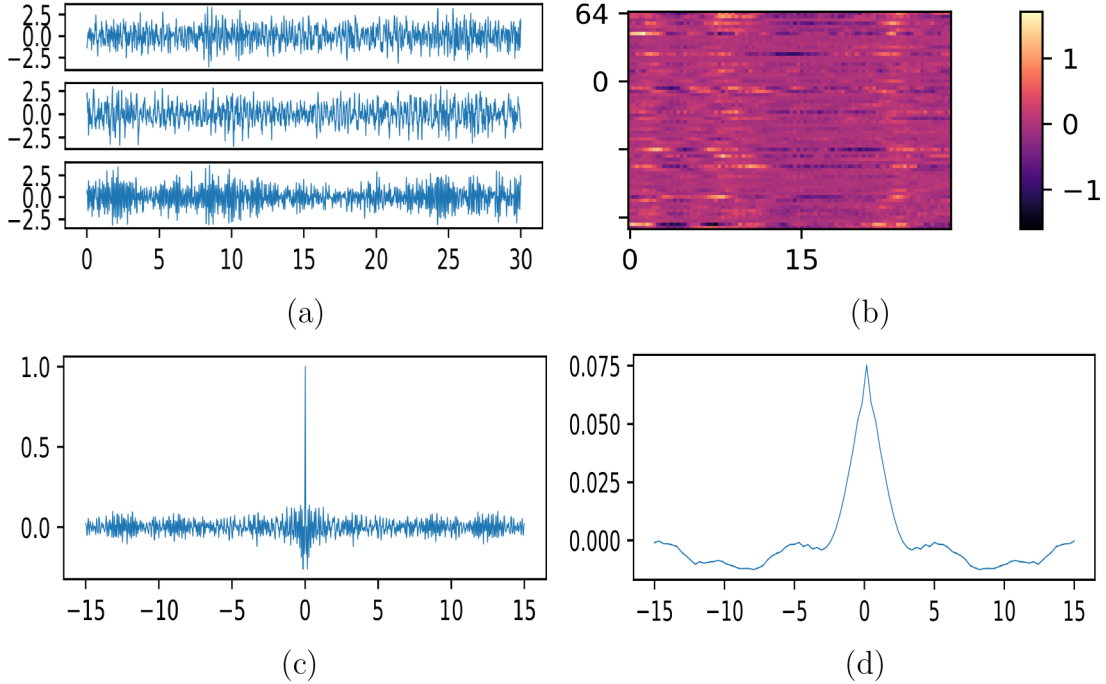


Fig. 3: Autoencoder noise sample 1 (a) three-channel waveform, (b) latent space representation, (c) waveform Autocovariance, (d) latent space Autocovariance. Note the relative lack of order in the latent space representation compared to the earthquake examples, and the weak autocovariance profile.

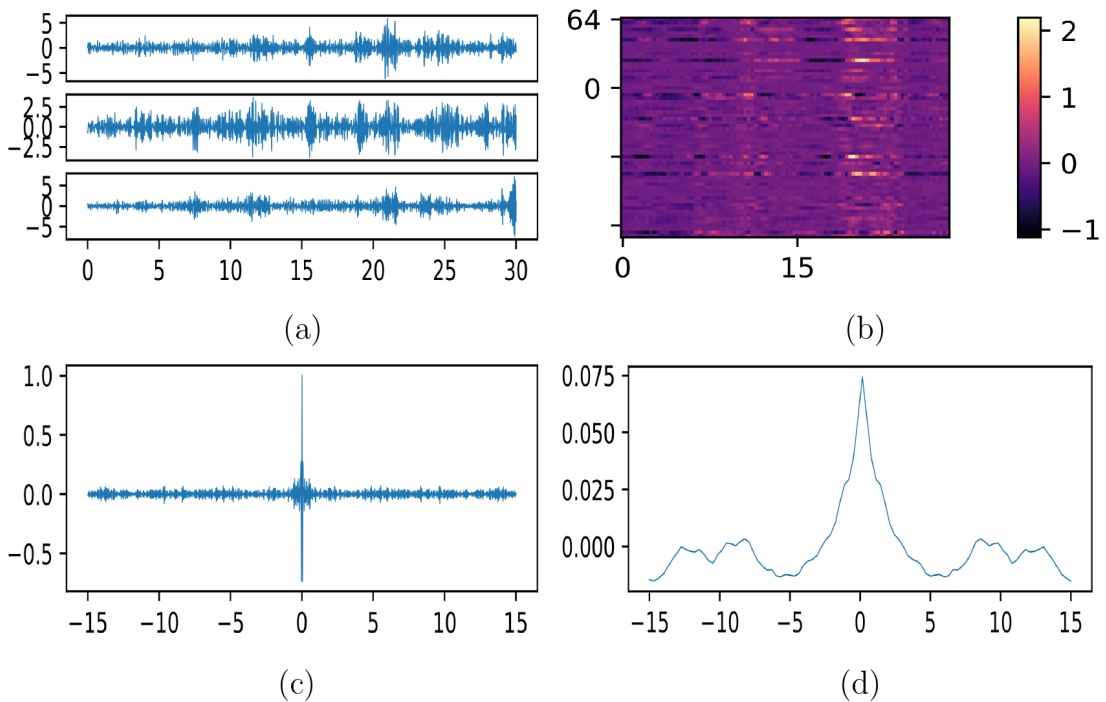


Fig. 4: Autoencoder noise sample 2 (a) three-channel waveform, (b) latent space representation, (c) waveform Autocovariance, (d) latent space Autocovariance. We have multiple plots for the latent space representation, each corresponding to a separate autoencoder head, after applying the projection maps described in the text. Note the clean “temporal phase transitions” in the latent space, despite the relative weakness of the signal, and the resulting strong covariance profile.

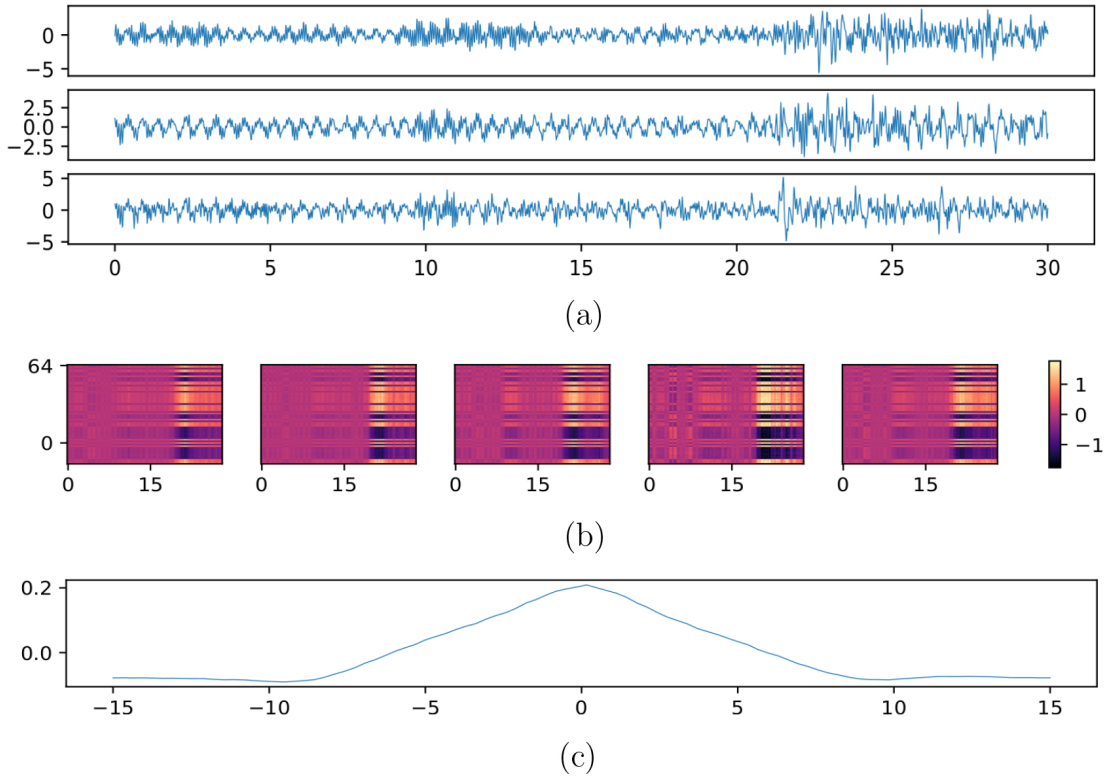


Fig. 5: Autoencoder ensemble earthquake sample 1 (a) three-channel waveform, (b) latent space representations for ensemble members, (c) mean latent space Cross-covariance.

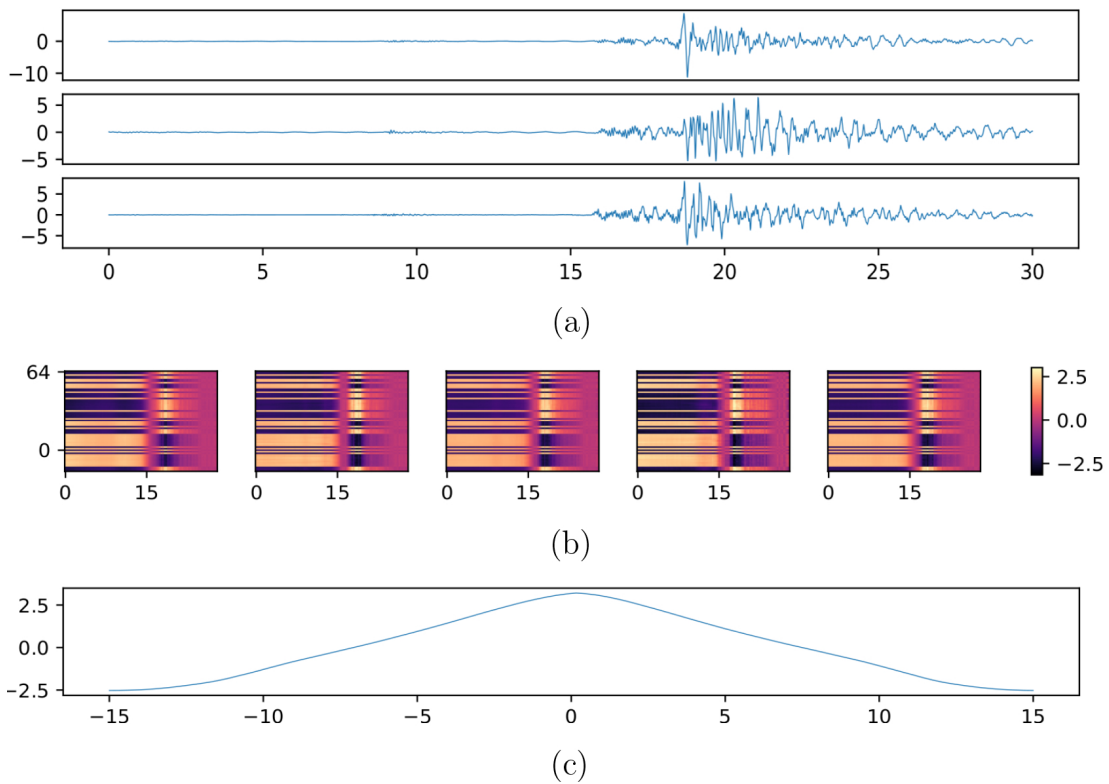


Fig. 6: Autoencoder ensemble earthquake sample 2 (a) three-channel waveform, (b) latent space representations for ensemble members, (c) mean latent space Cross-covariance.

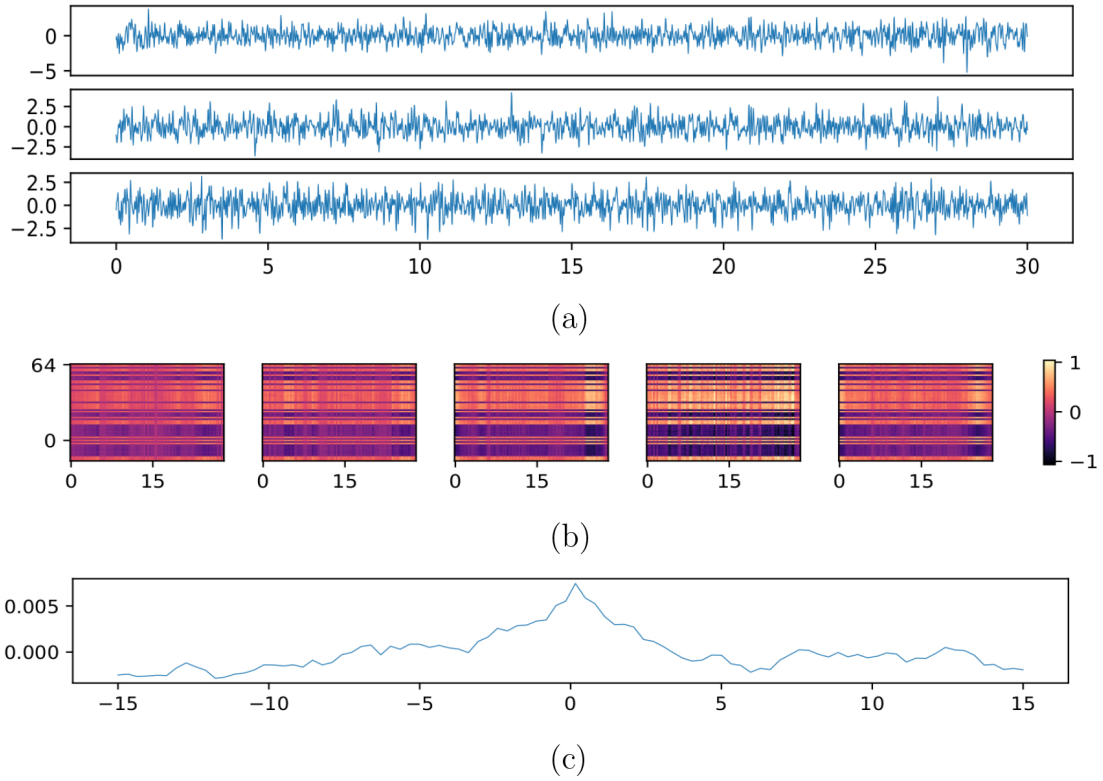


Fig. 7: Autoencoder ensemble noise sample 2 (a) three-channel waveform, (b) latent space representations for ensemble members, (c) mean latent space Cross-covariance. Note the lack of clean patterns in the latent space representation and the resulting weak covariance profile.

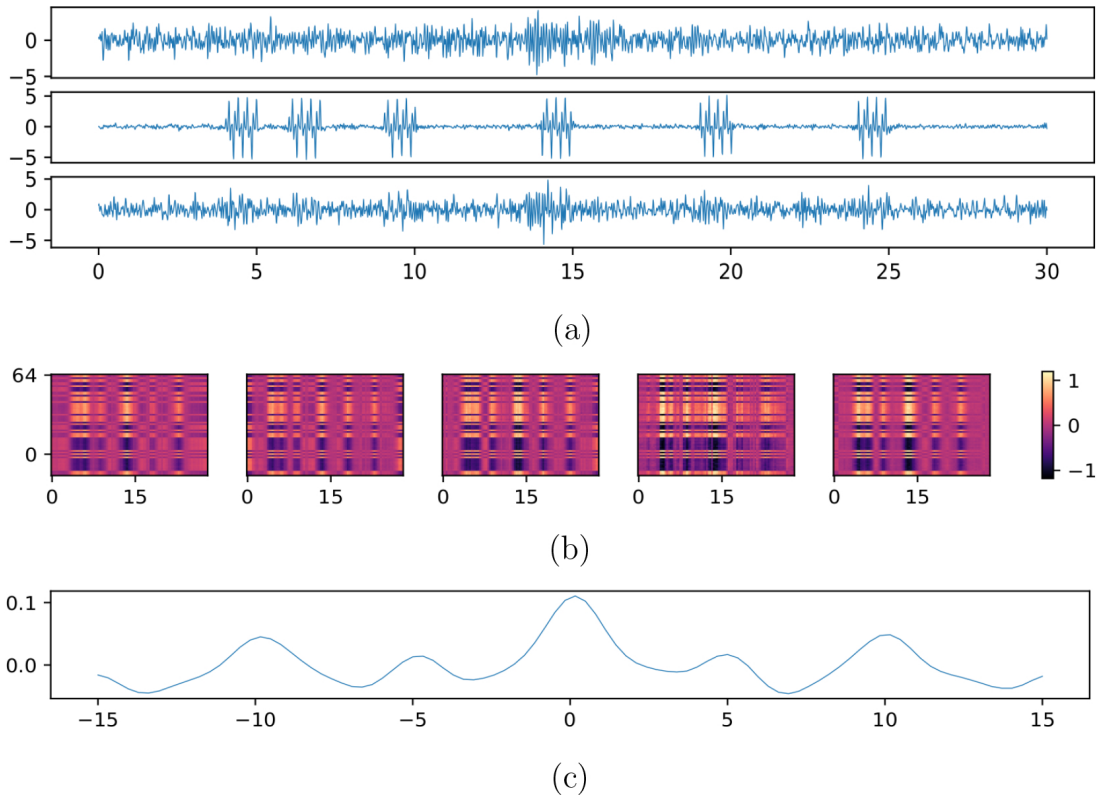


Fig. 8: Autoencoder ensemble noise sample 1 (a) three-channel waveform, (b) latent space representations for ensemble members, (c) mean latent space Cross-covariance. This example is labeled as noise in the dataset, but the method seems to pick up some cleanish patterns in the latent space representation. The interesting behavior in the waveform may indicate a tremor type event.

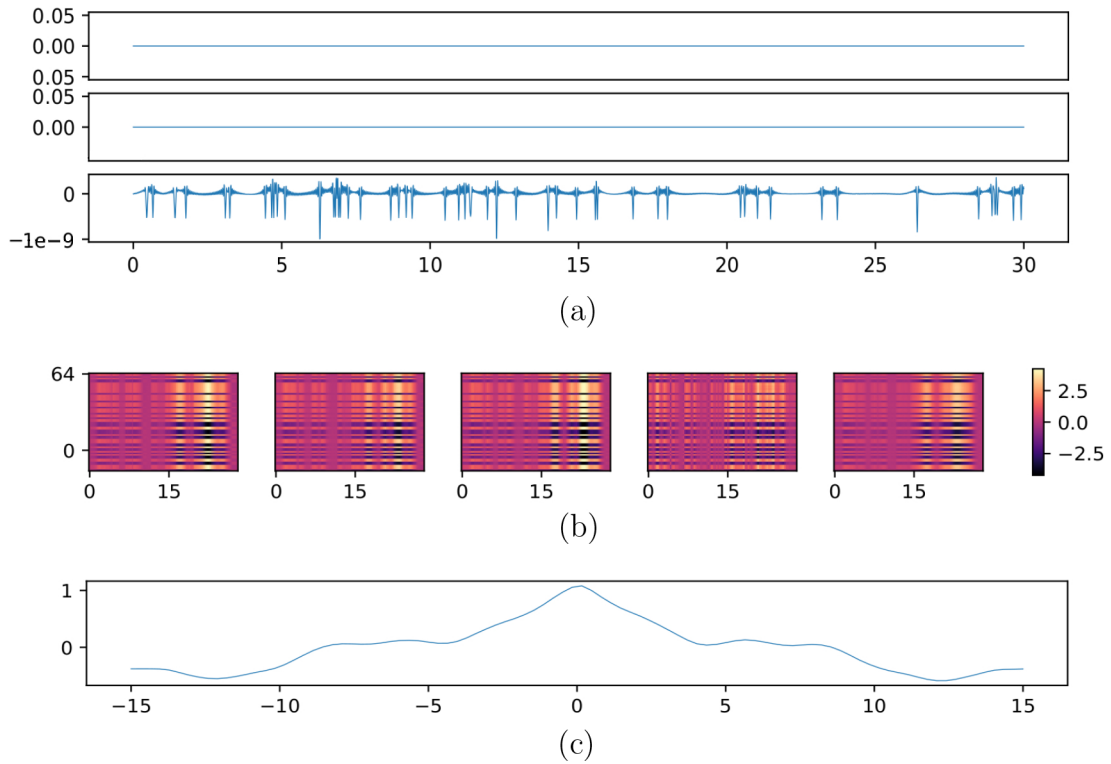


Fig. 9: Autoencoder ensemble noise sample 3 (a) three-channel waveform, (b) latent space representations for ensemble members, (c) mean latent space Cross-covariance. This waveform is mostly zero, but has some low-level spiky noise likely due to quantization errors. The waveform picks cleanish temporal patterns, and the resulting covariance profile is quite strong. This type of (easily identifiable) glitches seem to fool the method into giving false positives.

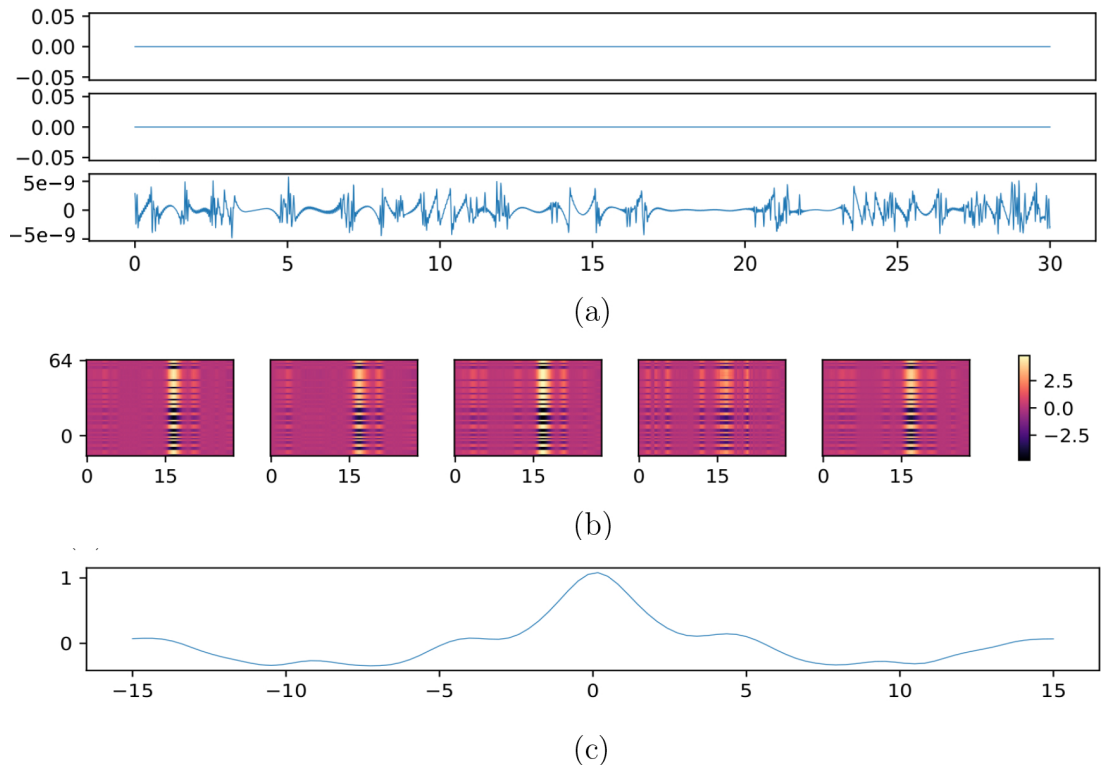


Fig. 10: Autoencoder ensemble noise sample 4 (a) three-channel waveform, (b) latent space representations for ensemble members, (c) mean latent space Cross-covariance. Similar to Figure 9, this is mostly a flat waveform, with glitches likely due to quantization errors. Once again the method is fooled into giving a false positive.

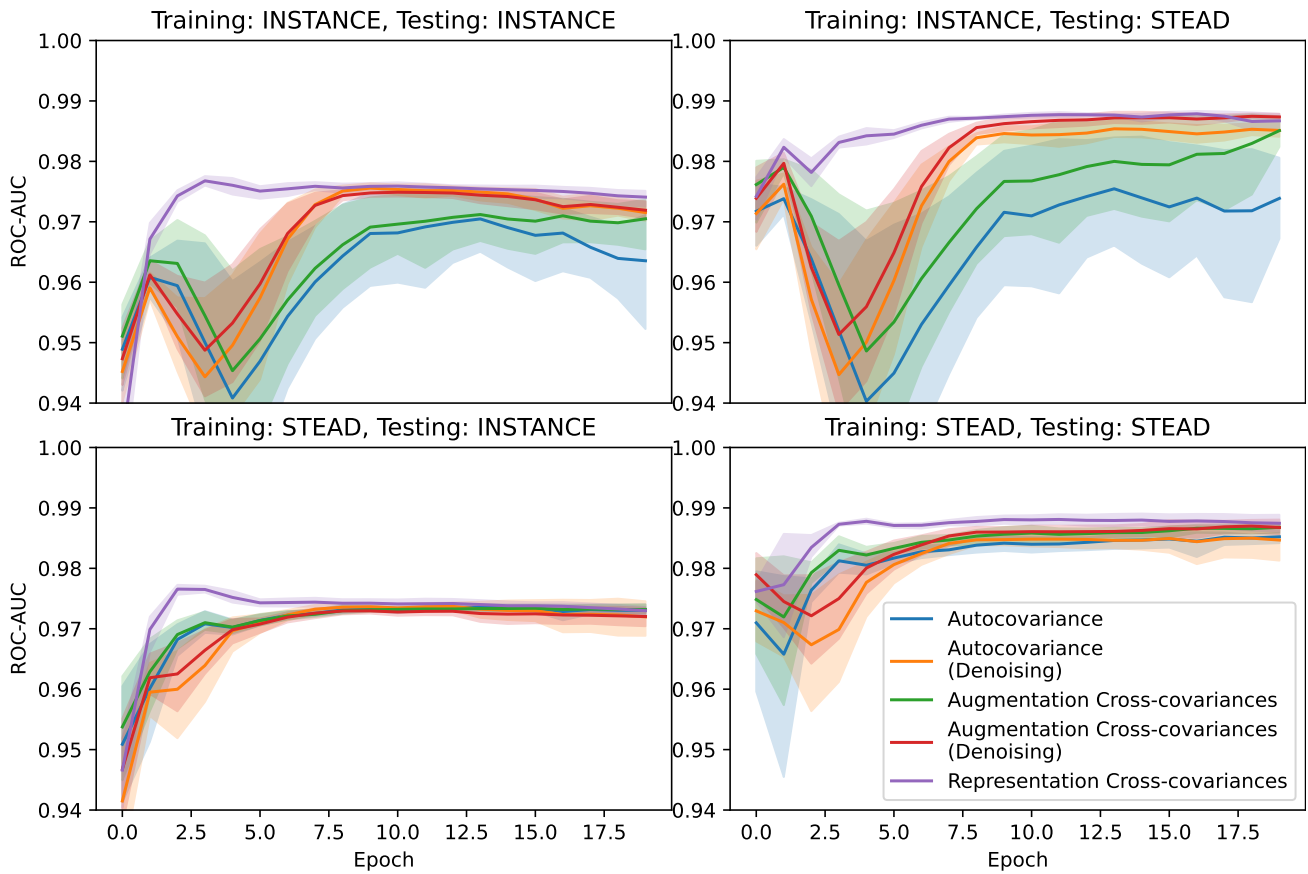


Fig. 11: ROC-AUC scores as a function of training duration.